

# Thermodynamic Analysis of High-Temperature Energy Storage Concepts Based on Liquid Metal Technology

Tim Laube,\* Luca Marocco, Klarissa Niedermeier, Julio Pacio, and Thomas Wetzel

Within the thermal energy storage (TES) initiative NAtional Demonstrator for IseNtropic Energy storage (NADINE), three projects have been conducted, each focusing on TES at different temperature levels. Herein, technical concepts for using liquid metal technology in innovative high-temperature TES systems are dealt with. This approach implies some challenges; first, the unit costs are relatively large which makes a reduction of the mass inventory necessary. Second, the high thermal diffusivity, which is beneficial in any heat exchanger unit, reduces the efficiency in a single-tank TES due to the fast degradation of the thermocline. These limitations can be overcome using a nonexpensive solid filler material, and, if properly designed, similar performance as in state-of-the-art molten salt systems can be obtained, while maintaining the advantage of operating at temperatures well beyond their upper limit. Optimization strategies are presented for a reference case including transient behavior of the whole system. The sensitivity of multiple parameters, e.g., porosity, particle size, and influence of storage capacity regarding the discharge efficiency, is investigated.

## 1. Introduction

The NAtional Demonstrator for IseNtropic Energy Storage (NADINE) initiative is a joint venture by University of Stuttgart, German Aerospace Center, and Karlsruhe Institute of Technology, aiming to establish an experimental research and development (R&D) infrastructure for developing and testing thermal energy storage (TES) technologies, in collaboration between academia and industry. Three complementary projects are conducted, working on novel TES materials, components, and systems. This work deals with the topics of the project focusing on liquid metal (LM)

technologies for TES in the high and very high temperature ranges.

Following an extensive deployment of renewable energy resources in recent years, storage solutions at utility or grid scale (GWh or even TWh) are required for a further sustainable energy system development. Among different technologies, pumped hydro energy storage systems represent the state of the art, with the largest installed capacity, but their potential is limited.<sup>[1]</sup> R&D projects on electrochemical energy storage, e.g., lithium-ion batteries, are currently on focus for automotive and household applications, although their large unit costs make them unsuited for large-scale storage.<sup>[2]</sup>

In contrast to the aforementioned technologies, TES systems are more suitable for large capacities at comparably low unit costs. Moreover, they can provide flexibility

for matching the supply and demand of heat in industrial processes. **Figure 1** shows the temperature levels of the heat demand in selected energy-intensive industries during one year in Europe, based on data from a previous study.<sup>[3]</sup>


Although the raw data do not allow for a more detailed analysis of the temperature level, three representative ranges are identified, as shown in Figure 1: low, high, and very high. Different technological solutions are required for implementing TES systems in these ranges, due to the stability limits of the materials.

As described in previous studies<sup>[4,5]</sup>, LMs such as lead, lead-bismuth eutectic (LBE), or sodium are attractive heat transfer fluids (HTFs) due to their beneficial thermophysical properties, in terms of high thermal conductivity and an extensive temperature range up to 1500 °C. Consequently, LMs are most convenient in applications at high thermal loads, as it was shown in nuclear and concentrated solar power (CSP) systems, see, e.g., a previous study.<sup>[6]</sup> In the past decades, extensive R&D work has been devoted to better understand the thermal-hydraulic behavior of these fluids, as well as the compatibility with structural materials, with significant progress in recent years.

An initial assessment of TES systems in a sodium-based CSP plant was presented by Niedermeier et al.<sup>[7]</sup> Aiming to reduce the LM inventory, a thermocline packed-bed TES was proposed after investigating different concepts for TES including sensible two-tank systems, latent and thermochemical storage systems. By using LMs as HTFs, higher storage temperatures can be achieved, what makes the application of advanced power cycles possible to reach higher efficiencies.<sup>[8]</sup> This study is based on the

T. Laube, Dr. K. Niedermeier, Dr. J. Pacio, Prof. T. Wetzel  
Karlsruhe Institute of Technology (KIT)  
Hermann-von-Helmholtz Platz 1, 76344 Eggenstein-Leopoldshafen,  
Germany  
E-mail: tim.laube@kit.edu

Prof. L. Marocco  
Department of Energy  
Politecnico di Milano  
via Lambruschini 4, 20156 Milan, Italy

 The ORCID identification number(s) for the author(s) of this article can be found under <https://doi.org/10.1002/ente.201900908>.

© 2019 The Authors. Published by WILEY-VCH Verlag GmbH & Co. KGaA, Weinheim. This is an open access article under the terms of the Creative Commons Attribution License, which permits use, distribution and reproduction in any medium, provided the original work is properly cited.

DOI: 10.1002/ente.201900908

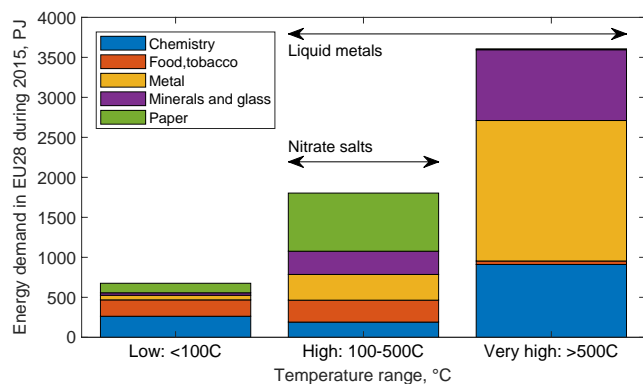


**Figure 1.** Yearly industrial heat demand for selected processes in Europe at several temperature levels (data taken from previous study<sup>[3]</sup>) and the operating range of two categories of HTFs: LMs and nitrate salts.

work of Niedermeier et al.<sup>[9]</sup> and investigates additional storage parameters and their influence on energy efficiency.

Beyond the electricity sector, a technological gap is shown in Figure 1 for industrial manufacturing processes operating at temperatures above 500 °C. Existing TES solutions are based on the sensible heat of a low-cost liquid with high heat capacity such as water, oil, and molten nitrate salts. These materials though are limited by their maximal temperature range. For high-temperature applications, molten nitrate salts such as the so-called solar salt (which represents the state-of-the-art TES systems in CSP plants) are not suitable beyond 600 °C<sup>[10]</sup> and thus cannot cover the range of interest for metallurgical, chemical, glass, and ceramic industries which could benefit from TES. For example, the exhaust gases leaving the electric arc furnace during scrap preheating in the steel manufacturing process reach an average temperature level of 1200 °C.<sup>[11]</sup> A similar level of 1300 °C can be found in the exhaust gases during glass manufacturing.<sup>[12]</sup>

The physical properties of several HTFs suitable for  $T > 600$  °C, including LMs, salts, and gases, are shown in Table 1. A high thermal conductivity and low viscosity are the main comparative advantages of LMs.

This work is structured as follows. In Section 2, the dual-media thermocline energy storage system and its mathematical description are given. A reference scenario is introduced in Section 3, and the results of a parametric study for the main aspects of the TES are presented in the Section 4. The concluding remarks are summarized in Section 5, including an outlook on the experimental program associated with NADINE.

## 2. Proposed System

Considering the relatively low specific volumetric heat capacity ( $\rho \times c_p$ ) of LMs, see Table 1, it is more cost effective to follow a dual-media approach with a thermocline storage tank partially filled with a solid material.<sup>[7]</sup> A TES system with such a thermocline storage tank is shown in Figure 2.

The LM coolant transports the heat from its source to the storage tank, where a thermal stratification (thermocline) is established, and eventually to the final heat sink. Four valves are required for turning the flow direction and switching from the charging to discharging mode with one single pump. During charging, valves V1 + V2 are open and V3 + V4 are closed: hot fluid enters the storage tank at the top and cold fluid exits at the bottom. The opposite setup (V1 + V2 closed, V3 + V4 open) directs cold fluid to the bottom of the tank and the hot fluid exits at the top. In this arrangement, it is possible to place the main components (valves, pump) in the cold leg.

A central component is the storage tank itself, partially filled with a low-cost solid material. For simplicity of modeling, the solid phase is represented as a homogeneous, monodisperse distribution of spheres with a diameter  $d$ , presumably much smaller than the tank diameter  $D$ . The Sauter mean diameter, that is, the

**Table 1.** Comparison of thermo-physical properties of several HTFs at 700 °C.

Fluid	Melting point ( $T_{\text{melt}}$ ) [°C]	Heat capacity ( $c_p$ ) [J kg <sup>-1</sup> K <sup>-1</sup> ]	Density ( $\rho$ ) [kg m <sup>-3</sup> ]	Volumetric capacity ( $\rho \times c_p$ ) [kJ m <sup>-3</sup> K <sup>-1</sup> ]	Thermal conductivity ( $\lambda$ ) [Wm <sup>-1</sup> K <sup>-1</sup> ]	Dynamic viscosity ( $\mu$ ) [mPa s]	Reference
<b>Liquid metals</b>							
Sodium (Na)	98	1256	798	1002.3	57.5	0.18	[13]
Lead–bismuth eutectic (LBE)	125	138	9807	1353.4	16.8	1.1	[14]
Pure lead (Pb)	327	141	10 196	1437.6	19.9	1.4	[14]
Tin (Sn)	232	282	6650	1875.3	32.0	1.1	[15]
<b>Reference solar salt (at 565 °C)</b>							
NaNO <sub>3</sub> –KNO <sub>3</sub>	228	1540	1730	2664.2	0.55	1.1	[16]
<b>Advanced salts</b>							
ZnCl <sub>2</sub> –NaCl–KCl	204	900	1977	1779.3	0.29	4.2	[17]
MgCl <sub>2</sub> –KCl	426	1150	1660	1909	0.50	5.0	[18]
Na <sub>2</sub> CO <sub>3</sub> –K <sub>2</sub> CO <sub>3</sub> –Li <sub>2</sub> CO <sub>3</sub>	398	1612	1848	2979	0.47	5.9	[19]
<b>Gases</b>							
Air (1 bar)	n.a.	1136	0.36	0.4	0.07	0.04	[20]
Steam (1 bar)	0	2273	0.22	0.5	0.09	0.04	[20]

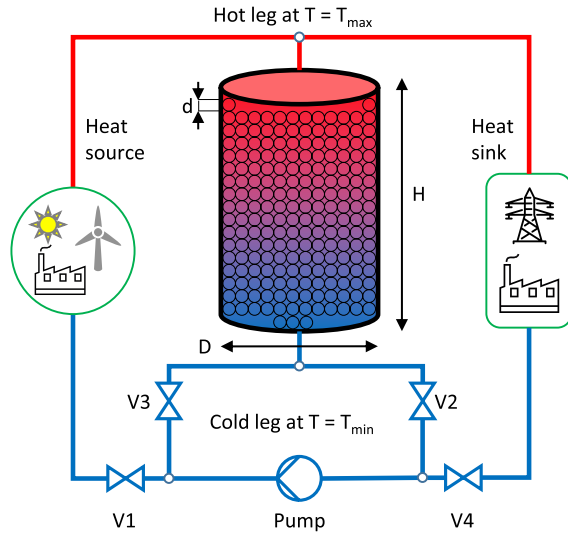


**Figure 2.** Flow scheme of TES based on single-tank thermocline.

size of an equivalent sphere having the same volume-to-surface area as the entire distribution, can be used as a representative of  $d$  for the general case.

In this setup, a temperature profile is established, where the upper region is hotter than the lower one. The evolution of this temperature profile determines the overall performance of the TES. For its evaluation, the model presented later is used.

### 2.1. Mathematical Description

A general formulation of this problem would require a 3D and transient representation of the energy balance in the particles, as well as a distributed mass, momentum, and energy conservation analysis in the fluid. This can be simplified with some assumptions, their validity determining the model accuracy.

First, a plug flow is considered, which can be obtained with a proper distributor design, and is usually observed in vessels with large  $D/d$  ratios.<sup>[21]</sup> Schlünder and Tsotsas<sup>[21]</sup> give an empirical correlation to calculate the ratio of the velocity  $u_0$  normalized with its mean value  $\bar{u}_0$  and the coefficients  $K$  and  $P$  as functions of  $D/d$ .

$$\frac{u_0}{\bar{u}_0} = \frac{K + \left(\frac{D}{d}\right)^P \frac{P+2}{2}}{K+1} \quad (1)$$

However, it has to be mentioned that the decrease in velocity close to the tank wall is neglected in this correlation. The maximum value for the cases in this work was smaller than 1.6% with the majority of cases with a deviation considerably smaller than 1%. Further assuming constant physical properties, it is not necessary to solve the continuity equation, and the superficial velocity is equal to the value  $u_0$  at the inlet.

Second, having assumed a plug flow, it is not relevant to solve the momentum equation, and the global pressure drop can be estimated by an empirical correlation, like Equation (2), proposed by Ergun,<sup>[22]</sup> based on early experimental data in monodisperse particle distributions ( $\epsilon < 0.74$ ). It shows a strong influence of the porosity ( $\epsilon$ ) and can be used for calculating the pressure drop.

$$\frac{\Delta p}{H} = 150 \frac{(1-\epsilon)^2 \mu_f \times u_0}{\epsilon^3 d^2} + 1.75 \frac{(1-\epsilon) \rho_f \times u_0^2}{\epsilon^3 d} \quad (2)$$

This correlation is valid in the range of  $3 < Re_p < 10^4$  according to Stieß.<sup>[23]</sup> with the particle Reynolds number  $Re_p = \rho_f \times u_0 \times d / \mu_f$ . The pressure drop was not considered in this article as a potential loss of efficiency because the order of magnitude is of minor influence compared with the thermal power of storage. This was already shown in a previous work by Niedermeier et al.<sup>[9]</sup>

Third, the transient energy balance is studied with a two-phase, 2D (2P-2D) model including intraparticle diffusion. For the continuous fluid phase, Equation (3) represents the temperature distribution as a function of the axial coordinate in the vessel  $x$ , the radial coordinate in the vessel  $r$  and the time  $t$ , with the accumulation and convective terms on the left-hand side and the diffusion and source terms on the right-hand side.

$$\begin{aligned} \epsilon \rho_f c_{p,f} \left( \frac{\partial T_f}{\partial t} + \frac{u_0}{\epsilon} \frac{\partial T_f}{\partial x} \right) = \epsilon \lambda_f \frac{\partial^2 T_f}{\partial x^2} + \dots \\ + \epsilon \lambda_f \left( \frac{\partial^2 T_f}{\partial r^2} + \frac{1}{r} \frac{\partial T_f}{\partial r} \right) + \dots \\ - h_V (T_f - T_{s,edge}) \end{aligned} \quad (3)$$

It should be noted that the same effective thermal conductivity ( $\epsilon \lambda_f$ ) is considered in Equation (3) for both radial ( $r$ ) and axial ( $x$ ) directions. A contribution by thermal diffusion in the solid phase is not included in Equation (3) because  $\lambda_s \ll \lambda_f$ , and, for spheres, there is only point contact between particles. The source term in Equation (3) indicates the interaction between both fluid and solid phase, given by a volumetric heat transfer coefficient ( $h_V$ ) and the temperature difference. Empirical correlations are available for the surface convective heat transfer ( $\alpha$ ) for flow around a sphere, normally in terms of the nondimensional Nusselt number ( $Nu = \alpha \times d / \lambda_f$ ). These can be adapted for  $h_V$  considering the specific surface area density as in Equation (4).

$$h_V = \alpha \times \frac{6(1-\epsilon)}{d} = Nu \times \frac{\lambda_f}{d} \times \frac{6(1-\epsilon)}{d} \quad (4)$$

The empirical correlation proposed by Wakao and Kaguei<sup>[24]</sup>, given by Equation (5), is widely used for calculating the mean Nusselt number in a packed bed, although it is strictly only valid for gases ( $Pr = c_{p,f} \times \mu_f / \lambda_f \approx 0.7$ ).

$$Nu = 2 + 1.1 \times Re_p^{0.6} \times Pr^{1/3} \quad (5)$$

A comparison of several Nusselt-correlations for molten salt was presented by Xu et al.<sup>[25]</sup>, concluding that the differences, in the case of salts, are minor. Moreover, considering the low Reynolds numbers in the reference scenarios (Section 3) and low Prandtl number of LMs, Equation (5) leads to values close to the laminar limit. Thus, in this work, a constant value of  $Nu = 2$  is used.

Furthermore, initial and boundary conditions are defined for  $T_f$  as in Equation (6). An initial temperature profile is defined (Equation 6a), as well as inlet conditions at  $x = 0$  (Equation 6b). Zero-gradient conditions are imposed at both the outlet  $x = H$  (Equation 6c) and the center line  $r = 0$  (Equation 6d). Thermal losses to the colder environment are considered at the outer wall with an overall heat transfer coefficient ( $h_W$ ), including the characteristics of the insulation layer (Equation 6e).

$$\text{At } t = 0: T_f = T_0(x, r) \quad (6a)$$

$$\text{At } x = 0: T_f = T_{in}(t) \quad (6b)$$

$$\text{At } x = H: \frac{\partial T_f}{\partial x} = 0 \quad (6c)$$

$$\text{At } r = 0: \frac{\partial T_f}{\partial r} = 0 \quad (6d)$$

$$\text{At } r = D/2: -\lambda_f \frac{\partial T_f}{\partial r} = h_w(T_f - T_{amb}) \quad (6e)$$

For the distributed solid phase, spherical symmetry can be assumed, leading to the energy balance as in Equation (7) expressed in the radial coordinate  $\gamma$ .

$$\rho_s c_{p,s} \frac{\partial T_s}{\partial t} = \lambda_s \left( \frac{\partial^2 T_s}{\partial \gamma^2} + \frac{2}{\gamma} \frac{\partial T_s}{\partial \gamma} \right) \quad (7)$$

Equation (7) does not include a source term, only the accumulation term on the left-hand side and the diffusion term on the right-hand side. This information is included in the initial and boundary conditions. Initially, the solid is assumed to have the same temperature as the surrounding fluid (Equation 8a), and zero gradient is imposed at the center (Equation 8b). The heat exchange with the fluid phase is represented by the boundary condition at the edge (Equation 8c).

$$\text{At } t = 0: T_s = T_f(x, r) \quad (8a)$$

$$\text{At } \gamma = 0: \frac{\partial T_s}{\partial \gamma} = 0 \quad (8b)$$

$$\text{At } \gamma = d/2: -\lambda_s \frac{\partial T_s}{\partial r} = \alpha(T_f - T_{s,edge}) \quad (8c)$$

Here it is relevant to recall again that the thermal conductivity of LMs is much higher than for other fluids (see Table 1) and also for the candidate solid materials. As a consequence the Biot number ( $Bi = Nu \times \lambda_f / \lambda_s$ ) is large and thus the solid phase cannot be approximated as a lumped capacitance, the differential Equation (7) must be solved instead. For other fluids, e.g., solar salt, such simplification is acceptable.

The energy equation (Equation (3) and (11)) is discretized using a second-order Crank–Nicolson scheme for time discretization, a central difference scheme for diffusive, and an upwind scheme for advective terms. They are solved in Matlab using the finite volume method.

## 2.2. Performance Criterion

Various figures of merit have been proposed in the literature for the performance of dual-media thermocline TES, see, e.g., an overview by Haller et al.<sup>[26]</sup> In general, these can be divided into first-law (energy) and second-law (exergy, entropy) types of efficiencies. In this work, a first-law type of efficiency is used to evaluate the system.

In an ideal storage system, the cold and hot regions would be perfectly separated without heat losses, and all the thermal energy ( $Q$ ) charged into it can be discharged at the same

temperature level. In practice, a performance degradation can occur due to internal thermal diffusion inside the tank, as well as heat losses to the environment. For representing these effects, the cycle efficiency ( $\eta \leq 1$ ) is defined as shown in Equation (9).

$$\eta = \frac{Q_{dis}}{Q_{chg}} = \frac{\int_0^{t_{dis}} \dot{m}_f \times c_{p,f} (T_{out} - T_{min}) dt}{\int_0^{t_{chg}} \dot{m}_f \times c_{p,f} (T_{max} - T_{min}) dt} \quad (9)$$

In the parametric study in Section 4, only a discharge efficiency is used with the constant  $Q_{chg}$  (see Table 2). It becomes clear from Equation (9) that the value of  $\eta$  depends on the characteristics of the storage cycle, namely, the charging and discharging times ( $t_{chg}$  and  $t_{dis}$ ). From the point of view of an energy balance, if losses to the environment can be neglected, all charged energy can eventually be discharged, leading to  $\eta \rightarrow 1$  for  $t_{dis} \rightarrow \infty$ . This definition is not practical because the discharge outlet temperature ( $T_{out}$ ) decreases when the thermocline region reaches the top. Instead, it is considered that the discharged energy is *useful* only if it exceeds a certain threshold value, and thus, for the assessment of the efficiency in Equation (9), the discharge time is limited to a value  $t_{dis,ref}$ . In this work, the integration is stopped when the nondimensional temperature at the outlet ( $\Theta_{out}$ ) reaches 0.8, as shown in Equation (10).

$$\Theta = \frac{T - T_{min}}{T_{max} - T_{min}} \Rightarrow \Theta_{out}(t_{dis,ref}) = 0.8 \quad (10)$$

**Table 2.** Main parameters for the reference TES system NADINE. All listed physical properties are evaluated at the mean temperature.

Parameter	Symbol	Value
<b>Process parameters</b>		
Minimum temperature	$T_{min}$	350 °C
Maximum temperature	$T_{max}$	750 °C
Thermal power	$\dot{Q}$	1.0 MW
Charging time	$t_{chg}$	3600 s
Discharging time	$t_{dis}$	3600 s
<b>Storage vessel</b>		
Height	$H$	2.658 m
Diameter	$D$	1.329 m
Porosity	$\varepsilon$	0.26
Storage capacity	$Q_{chg}$	1.0 MWh
<b>Fluid</b>		
		Lead (Pb)
Mean density	$\rho_f$	1033 kg m <sup>-3</sup>
Mean heat capacity	$c_{p,f}$	143.9 J kg <sup>-1</sup> K <sup>-1</sup>
Thermal conductivity	$\lambda_f$	18.25 Wm <sup>-1</sup> K <sup>-1</sup>
Viscosity	$\mu_f$	1.67 mPa s
Mass flow rate	$\dot{m}$	17.37 kg s <sup>-1</sup>
<b>Solid</b>		
		Quartzite
Density	$\rho_s$	2640 kgm <sup>-3</sup>
Heat capacity	$c_{p,s}$	1050 J kg <sup>-1</sup> K <sup>-1</sup>
Thermal conductivity	$\lambda_s$	2.5 Wm <sup>-1</sup> K <sup>-1</sup>
Particle diameter	$d$	15 mm

It should be noted that the value of 0.8 is arbitrary and can be adjusted to the study of a specific process. This definition allows a direct comparison with a state-of-the-art two-tank system which, working within the same acceptable temperature range, would have an ideal performance (no mixing) and an efficiency of  $\eta = 1$ .

Other energy-based efficiencies have been proposed relative to the maximum thermal energy which can be stored in the tank, thus representing an economic utilization factor for the materials. Their analysis is beyond the scope of this article. For further reference, see, e.g., previous studies<sup>[27,28]</sup>.

Similarly, the width of the thermocline region can be defined based on the nondimensional temperature  $\Theta$ . Arbitrary threshold values can be defined for distinguishing between the hot ( $\Theta \approx 1$ ), cold ( $\Theta \approx 0$ ), and thermal mixing regions. Here, the thermocline region is defined where  $0.05 \leq \Theta \leq 0.95$ . These values are selected with the perspective of comparison with experimental data, see Section 5. With these considerations, a nondimensional width of the thermocline region  $\zeta$  is defined, as in Equation (11).

$$\zeta = \frac{\Delta x|_{0.05 \leq \Theta \leq 0.95}}{H} \quad (11)$$

### 3. Reference Scenario

A preliminary validation of the model described in Section 2.1 has been presented by Niedermeier et al.<sup>[9]</sup> In the absence of currently available experimental data with LMs, published experiments with solar salt and thermal oil, as given in previous studies<sup>[29,30]</sup>, have been used. Good agreement with the experimental data has been obtained, with minor differences attributed to uncertainties and challenges in the experiments, as well as simplifications of the mathematical model to reduce computational effort, e.g., constant physical properties. With a successful preliminary validation (i.e., not yet for LMs), this model can be used for studying a reference scenario with LMs, as follows.

The selected reference scenario is given by the planned demonstration facility NADINE, with parameters as shown in Table 2. In Section 4, the results of a parametric study are detailed, and trends of optimization are identified.

In the reference scenario considered here, the system is initially discharged (i.e., at  $T = T_{\min} \rightarrow \Theta = 0$ ) and is charged at a constant mass flow rate ( $\dot{m}$ ) as required for transferring the rated power for the given temperatures, during a time  $t_{\text{chg}}$ , and it is subsequently discharged at the same mass flow rate and during the same time:  $t_{\text{chg}} = t_{\text{dis}}$ .

It is important to note that stand-by periods and heat losses are not considered in this analysis. This is a simplification for understanding the effects of other parameters first. For an outlook on the analysis of stand-by periods, see Section 5.

For a given TES setup, many different operation strategies can be followed, depending on the overall integration in a larger system, as recently highlighted by Ortega-Fernández et al.<sup>[28]</sup> **Figure 3** and **4** show the results for a cyclic operation with fixed time intervals. In other words, the simulation of the TES system is left to run until  $t = t_{\text{chg}}$  for charging and until  $t = t_{\text{dis}}$  for discharging, independently of the results.

In **Figure 3**, the temperature distributions in the tank are displayed at selected times, namely, at the end of each step

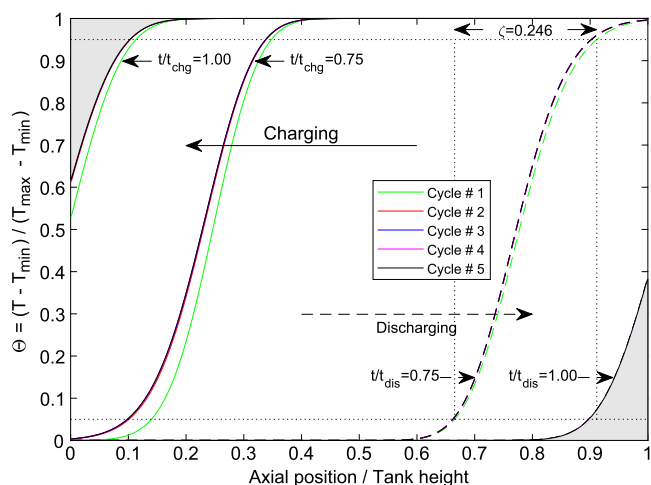


**Figure 3.** Temperature profiles at selected times for a cyclic charging and discharging process without stand-by.

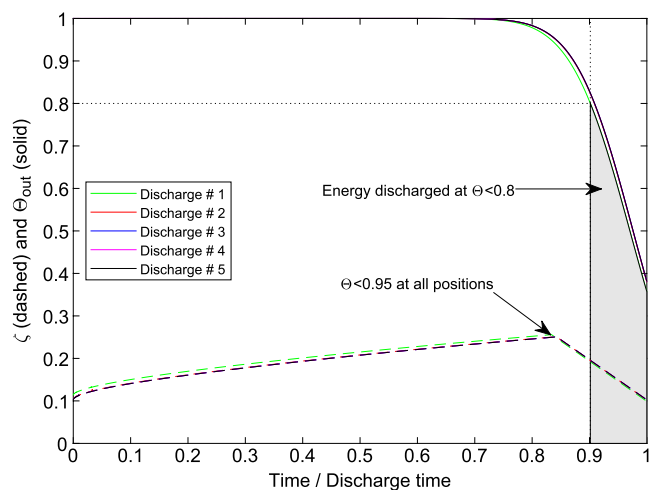


**Figure 4.** Evolution in time of the thermocline width and outlet temperature during the discharging process without stand-by.

(charging: solid lines, discharging: dashed) and (arbitrarily) at 75% of the time, for five cycles (different colors).

Several conclusions can be derived from **Figure 3**. First, similar results are obtained for all cycles. Minor differences are observed only for the first charging and discharging steps, because the initial condition was homogeneous. For all other cycles, the initial condition is the solution at the end of the previous cycle, and a stable cyclic behavior is soon established: differences are negligible after three cycles.

Second, the thermocline region is shown in **Figure 3** for  $t/t_{\text{chg}} = 0.75$  and  $t/t_{\text{dis}} = 0.75$ . The S-shape of these curves represents the deviation from an ideal case, where the separation between the cold and hot regions would be sharp as in a step function. Based on the definition given in Equation (11), the value of the thermocline nondimensional width  $\zeta$  is shown in **Figure 3**.

Third, when the charging or discharging processes are completed (i.e., at  $t = t_{\text{chg}}$  or  $t = t_{\text{dis}}$ ), the TES is not completely charged or discharged. This is a consequence of the temperature



profile: additional time is required to charge or discharge the TES completely ( $\Theta = 1$  or  $\Theta = 0$  at all positions). Alternatively, if the operation is constrained by time as considered in this work, some regions of the tank would not be completely utilized. These regions are marked in gray in Figure 3.

Figure 4 shows the evolution in time of the thermocline width  $\zeta$  and the outlet nondimensional temperature during the discharging process.

During an initial period, up to  $t/t_{\text{dis}} \approx 0.7$ , the TES can be discharged at its maximum temperature. Beyond this time, the thermocline region reaches the top, and the outlet temperature starts to decrease, i.e.,  $\Theta_{\text{out}} < 1$ . Eventually, the threshold value of 0.8 defined in Section 2.2 is reached, and the energy discharged afterward (region marked in gray) is considered as not useful. Alternatively, another optimized operation strategy could be defined, where the discharging process is stopped at that point.

Figure 4 shows that the width of the thermocline region increases with time until a maximum value is reached. The initial value corresponds to the state at the end of the previous charging process. Near the end of the discharging process, the thermocline region is partially pushed out of the domain and, based on the definition of  $\zeta$  given in Equation (11), is reduced. This is a particular feature of the operational strategy, which allows to start the next cycle with a smaller thermocline region and thus reach high efficiencies.

#### 4. Optimization: Parametric Study

Some relevant trends have been identified in a previous study by Niedermeier et al.<sup>[9]</sup> on the sensitivity of the overall performance with respect to several parameters, e.g., porosity,  $H/D$  ratio of the storage tank, and particle size.

Regarding the investment costs of a storage system, a low porosity can be preferred due to the lower market prices of filler material compared with LMs. In addition, with low porosity, the efficiency of storage increases. The filler particles limit the axial thermal conduction, resulting in a better separation of the cold and hot regions in the storage tank. The expansion of the thermocline region can be reduced what leads to a better stand-by performance.

In relative terms, the influence of the thermocline expansion can be minimized if a storage tank with a large height is used. For a given constant volume (capacity), this leads to high  $H/D$  ratios. Furthermore, high  $H/D$  ratios result in higher velocities of the HTF and consequently a better heat transfer with the solid particles.

Regarding the particle size, small particles are preferred to reduce the influence of heat conduction within the solid. Especially for large particles, the thermal resistance within the solid limits the heat transport between the HTF and the filler material, negatively impacting on the system performance.

This section builds up on these previous results and focuses on studying the effects of additional design parameters, namely, the storage capacity, discharge time, and selection of the HTF, along these aforementioned lines.

Consequently, three curves are shown for comparing several TES configurations in each study: 1) efficiency versus porosity, 2) efficiency versus  $H/D$ -ratio, and 3) efficiency versus particle size.

For simplicity, only the discharging step is calculated, assuming that the tank is fully charged ( $T = T_{\text{max}}$ ) as the initial condition at  $t = 0$ . All qualitative trends are also applicable for the complete cycle with both charging and discharging steps.

##### 4.1. Influence of the Storage Capacity

To investigate the influence of the storage capacity, two systems with a large difference in size and power are studied (otherwise with the same materials as shown in Table 2). The first one, called NADINE, is the reference for a laboratory setup, with the main parameters as shown in Table 2. A second one, here named INDUSTRIAL, is representative of the TES size of the Gemasolar CSP facility in Spain,<sup>[31]</sup> with a capacity of 1800 MWh and a larger discharge time of 15 h leading to a thermal power of 120 MW. These two configurations are compared in Figure 5. For comparison, the parameters shown in Table 2 are the same for both cases except of the thermal power and storage capacity. In addition, the dimensions of the storage vessel and consequently the mass flow rate of the fluid are scaled to the thermal power and storage capacity of each case.

All curves show a better performance, i.e., higher efficiency, for the larger industrial system. Due to the large height of the bigger tank, the impact of the thermocline expansion is weaker in relative terms, even at low  $H/D$  ratios. For the smaller NADINE system, a significantly higher sensitivity regarding particle size is observed. If the system is to be discharged quickly and the heat conduction in the solid is the limiting factor, then a large temperature difference is established, resulting in a lower efficiency.

##### 4.2. Influence of the Discharge Time

Following up on the last observation in Section 4.1, the effect of the discharging time is studied for the NADINE reference case with the parameters shown in Table 2. Figure 6 shows the results of increasing  $t_{\text{dis}}$  from the reference value of 1 h (NADINE 1h) up to 5 h (NADINE 5h).

In Figure 6a,b, that is considering the influences of the porosity and  $H/D$ -ratio while keeping other parameters constant, better results are observed for shorter discharging times. For larger values of  $t_{\text{dis}}$ , the influence of axial heat conduction and growing thermocline thickness lead to lower efficiencies, and this is most significant for high porosity due to the high conductivity of LMs.

On the contrary, Figure 6c shows a different trend: for larger discharging times, the influence of the particle size is less significant, i.e., the curves are less steep. A transition point is observed between 15 and 20 mm, where the curves of the cases with discharge times of  $t_{\text{dis}} = 1$  h and  $t_{\text{dis}} = 2$  h cross each other and the trend is reversed. To observe this trend more in detail, a further increase in particle size would be interesting; anyway then, the assumption of high ratios of  $D/d$  would not be fulfilled anymore, resulting in a decrease in model accuracy. For short discharge times, small particles are preferred, whereas for long discharge times, larger particles can lead to good results. An increase in particle size leads to a decrease in the heat transfer coefficient  $\alpha$  and the volumetric heat transfer coefficient  $h_V$ . Due to that the kinetics of heat transfer is deteriorated which becomes important for short discharge times. Large particle sizes can also

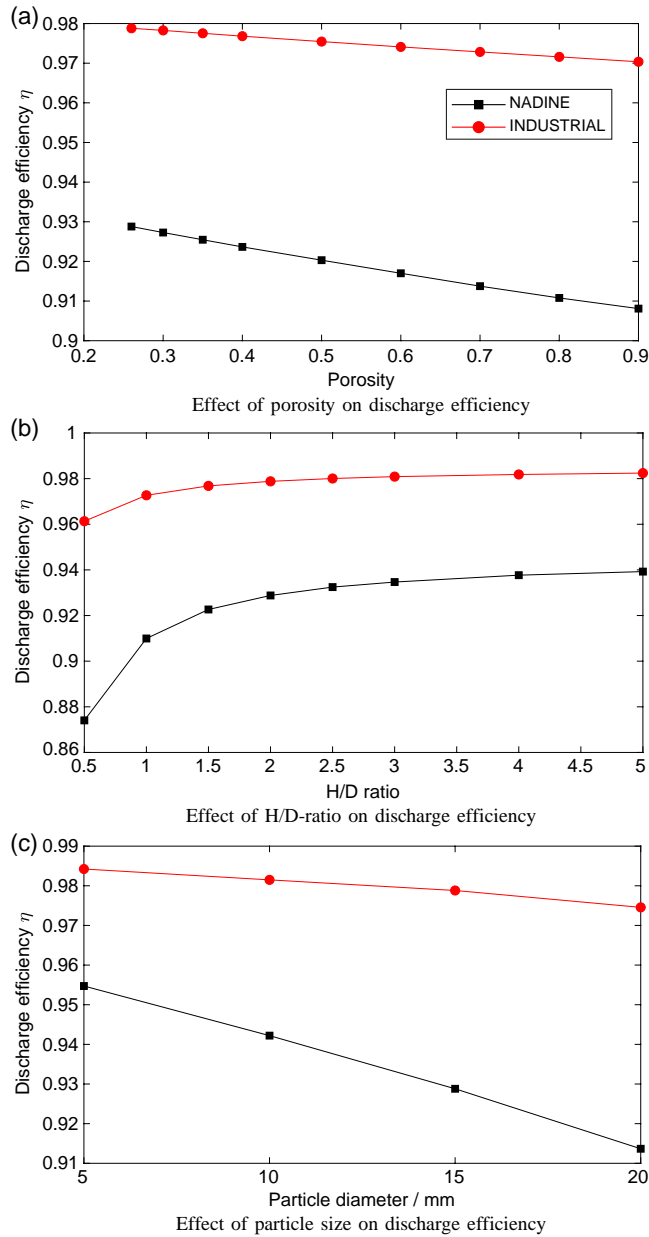


**Figure 5.** Effects of several parameters on the discharge efficiency of TES for different storage capacities.

be beneficial during stand-by periods, as they limit the axial heat conduction in the tank.

### 4.3. Influence of the Heat Transfer Fluid

To investigate the effect of the fluid physical properties in detail, the performance of a TES using different HTFs is studied for a reference case similar to the one shown in Table 2. Four fluids are considered: three LMs (Na, Pb, and LBE) are compared with solar salt, with the thermal properties corresponding to the mean temperature as shown in Table 3. As additional information, the Prandtl number ( $Pr_f$ ) is shown in Table 3.

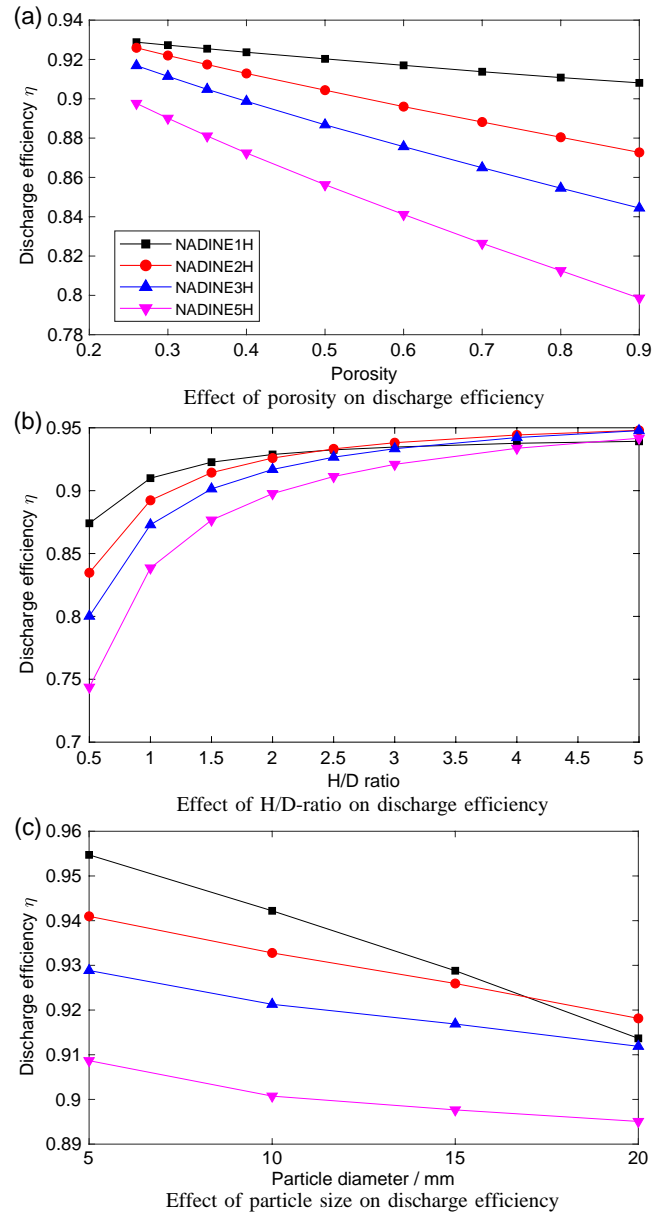


**Figure 6.** Effects of several parameters on discharge efficiency of thermal storage for different discharge times.

**Table 3.** Reference physical properties of four HTFs for comparison, each at the mean temperature.

Property	Na	Pb	LBE	Solar salt
$\rho_f$ [ $\text{kg m}^{-3}$ ]	829	10 388	10 001	1804
$c_{p,f}$ [ $\text{J kg}^{-1} \text{K}^{-1}$ ]	1256.8	143.9	140.2	1520.4
$\lambda_f$ [ $\text{Wm}^{-1} \text{K}^{-1}$ ]	64.85	18.25	15.03	0.53
$\mu_f$ [mPa s]	0.23	1.67	1.23	1.47
$Pr_f$ [-]	0.0044	0.0131	0.0115	4.236

For each HTF, the TES tank volume is scaled so that the thermal capacity is the same in each case (1.0 MWh). This was done by adapting the tank volume considering the porosity and the properties of the fluid and solid, as represented in Equation (12).

$$V = \frac{Q_{\text{chg}}}{(\rho \times c_p)_{\text{eff}}(T_{\text{max}} - T_{\text{min}})} \quad (12)$$

$(\rho \times c_p)_{\text{eff}}$  in Equation (12) is calculated with Equation (13). The tank height  $H$  and diameter  $D$  consequently can be calculated with the tank volume  $V$  and the  $H/D$ -ratio.

$$(\rho \times c_p)_{\text{eff}} = \rho_f c_{p,f} \varepsilon + \rho_s c_{p,s} (1 - \varepsilon) \quad (13)$$

The temperature range for solar salt is reduced to 300–600 °C, due to its stability limit. **Figure 7** shows the main results of this comparison.

The results for solar salt in **Figure 7** show a different trend that those for LMs. This difference can be explained by the much lower thermal conductivity of solar salt.

For solar salt, the efficiency increases with ascending porosity. In contrast to LMs, the heat conductivity of the solar salt is actually lower than that of the solid material itself (see **Table 2**). With a high porosity, the growth of thermocline through conduction in the solid is inhibited. This circumstance also explains the curves for the  $H/D$ -ratio: the impact is lower for solar salt due to the lower thermal conductivity.

The efficiency strongly decreases for large particles for all HTFs. Here the main limiting factor is the thermal conduction within the particles, and the sensitivity is higher for solar salt because a high heat flux at the interface cannot be imposed.

Comparing the results for the LMs with each other, it is observed that Pb and LBE behave nearly the same, as their properties are very similar. In all cases, a lower efficiency is observed for sodium. While its high thermal conductivity makes Na an attractive HTF, in this study, it leads to a large heat diffusion and growth of thermocline, resulting in a reduced efficiency. Furthermore, the heat transfer between the fluid and solid is mostly limited by thermal conduction in the particles; thus, there is no added value from the high  $\lambda_f$  of Na. The thermal properties of Pb and LBE are in this case better suited.

With these considerations, knowing that the thermal conductivity of sodium is too high and that of solar salt is too low, it is interesting to study whether an optimum value of  $\lambda_f$  exists. In an exercise of purely academic value, the thermal conductivity of these fluids is varied by a factor  $\lambda_f/\lambda_{f,\text{ref}}$  over a broad range, while keeping  $\rho_f$  and  $c_{p,f}$  and consequently the storage capacity constant. These results are presented in terms of the discharge efficiency in **Figure 8**. Although they do not have a direct practical meaning, because such artificial HTFs do not exist, they illustrate the underlying physical mechanisms well and shed light on possible optimization strategies for each case. Because the properties of Pb and LBE are similar, only Pb is considered here.

For each curve shown in **Figure 8**, an optimum value of  $\lambda/\lambda_{\text{ref}}$  is found, as indicated by the arrows. Although the exact value of this optimum factor is not directly relevant in practice (in principle, it depends also on other parameters shown in **Table 2**), it should be noted that it is lower than 1.0 for the LMs (Na, Pb) and larger than 1.0 for solar salt.

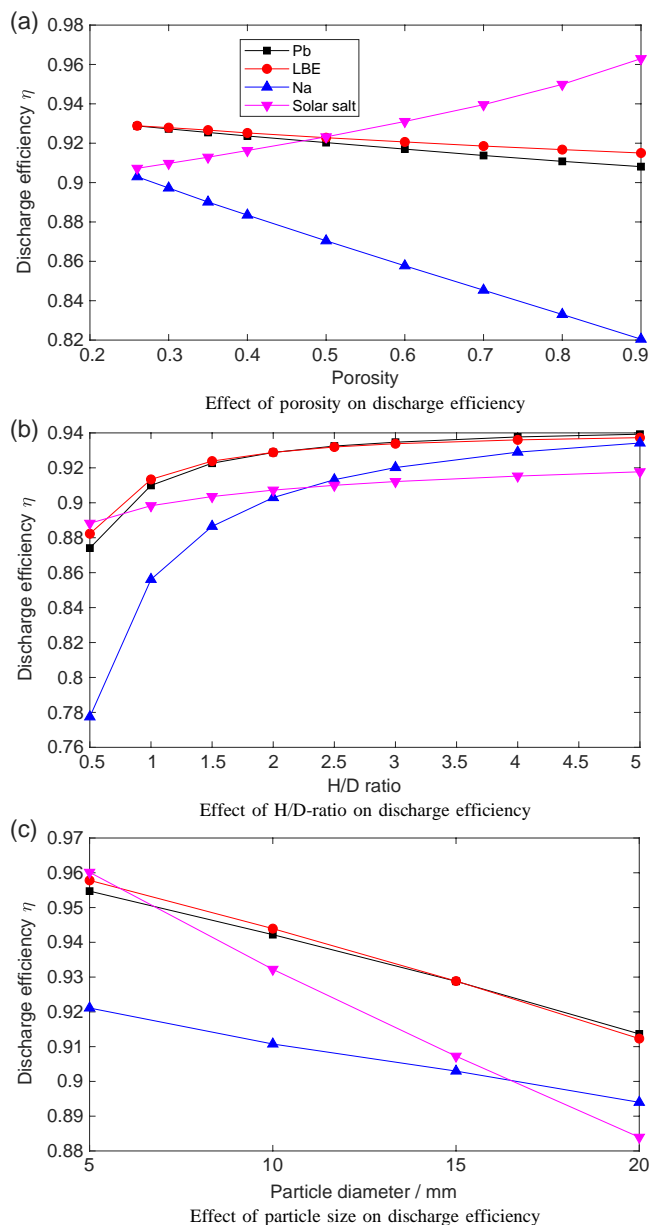


**Figure 7.** Effects of several parameters on the discharge efficiency of thermal storage for different HTFs.

In other words, the real thermal conductivity of solar salt is much lower than its optimum value, and the efficiency would increase if  $\lambda$  were larger than  $\lambda_{\text{ref}}$ . This is an indication that this system is limited by the heat transfer between HTF and solid particles. On the contrary, the thermal conductivity of LMs is larger than its optimum value, and the efficiency would increase if  $\lambda$  were smaller than  $\lambda_{\text{ref}}$ . This result indicates that the main factor limiting the performance of an LM-based TES is the internal heat diffusion within the HTF. For the case of Pb, the optimum is very close to the reference value, and the curve is predominantly flat in that region, indicating that a convenient balance between two effects (on the one hand, heat transfer between solid and HTF, and, on the other hand, internal heat diffusion) is established.



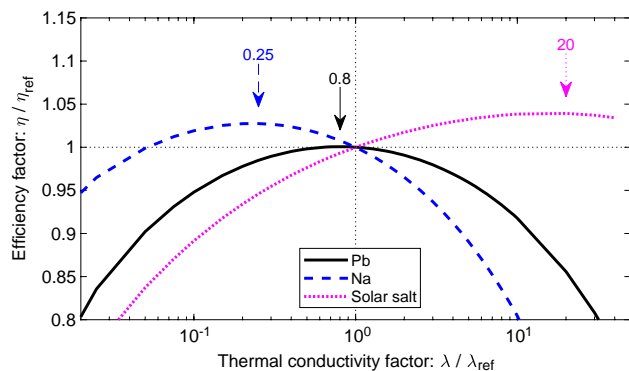


**Figure 8.** Discharge efficiency if the thermal conductivity  $\lambda$  of the HTF is multiplied by a factor,  $\lambda/\lambda_{\text{ref}}$ , for the reference scenario.

## 5. Conclusions

Large-scale TES systems can allow an extensive deployment of fluctuating renewable energy resources in both the electricity and the industrial heat sectors. The use of solar salt in CSP plants represents the state of the art up to 565 °C. For fully exploiting the higher temperature range, where a significant fraction of the energy demand is concentrated, innovative technological solutions are required.

In this context, LMs, such as sodium and lead alloys, present advantageous characteristics as HTFs for high-temperature applications. They are stable liquids in a broad temperature range and have a high thermal conductivity, which leads to efficient heat transfer performance in many geometries and configurations. Their use in TES systems is studied in this work.

Following cost considerations, a single-tank, dual-media approach is proposed. In this concept, the largest fraction of the heat capacity is provided by non-expensive solid particles, and the main role of LMs is to transport the heat. A mathematical description of the model is presented, along with some figures of merit for representing the system performance. In particular, the efficiency is defined in a way that allows a direct comparison with a two-tank system. This model has been preliminarily validated using literature data with solar salt as a HTF, as reported recently in a previous study by Niedermeier et al.<sup>[9]</sup>, in the absence of experimental data with LMs.

A reference scenario is studied, with technical parameters representative of the envisaged facility NADINE. An analysis of the temperature profile indicates that the key factor for improving the system performance is to obtain a thin thermocline region. For this, two physical processes are relevant: the heat diffusion along the tank axis and the heat transfer between HTF and solid particles.

Some optimization trends have been identified in the previous study by Niedermeier et al.<sup>[9]</sup> In particular, a low porosity, high H/D-ratio, and small particle sizes are preferred for increasing the system efficiency. In this work, the effects of the system size, discharge time, as well as selected HTF are studied along these lines. The first two effects indicate clear optimization strategies: better performance is obtained for larger systems and faster operation. These conditions lead to a more effective separation of cold

and hot regions and thus high round-trip efficiencies. Values as high as 95% are obtained, which is comparable with state-of-the-art two-tank systems using nitrate salts, while keeping the advantage of potentially extending the temperature range.

Regarding the effects of the properties of the HTF itself, four fluids are compared: Na, Pb, LBE, and solar salt. The best results are obtained for LBE and very similar ones for pure Pb. In an exercise of purely academic value, other artificial HTFs are studied, where the thermal conductivity of Na, Pb, and solar salts is multiplied by a factor in a broad range from 0.025 to 40. Although such HTFs are not real, this study indicates that an optimum value of  $\lambda$  exists. If  $\lambda$  is lower, then the system is limited by the heat transfer between HTF and solid particles, and if  $\lambda$  is larger, then the internal heat diffusion along the tank axis is the limiting factor. Incidentally, the optimum value of  $\lambda$  is close to the real value for Pb and LBE.

It is highlighted that experimental data on such a system with LMs are currently not available. The ongoing research program at KIT envisages a validation test in an existing LM (LBE) facility and the construction of a research infrastructure at demonstration scale within the NADINE initiative. This two-step experimental program shall demonstrate the postulated advantages of LMs as high-temperature HTFs and pave the way for the development of storage solutions based on this concept and their integration in industrial processes, beyond the current state-of-the-art application of TES in CSP plants.

The NADINE initiative shall serve both as demonstration facility and as test platform for investigating associated technological issues. Among others, strategies for minimizing losses during stand-by periods and integrating fluctuating processes on the supply or demand side shall be studied, as well as the compatibility with structural materials at high temperatures.

## Acknowledgements

This work was supported by the German Federal Ministry for Economic Affairs and Energy (BMWi) and the Projektträger Jülich (PtJ) in the frame of the collaborative project DESI-NADINE.

## Conflict of Interest

The authors declare no conflict of interest.

## Keywords

high temperatures, liquid metals, NADINE, thermal energy storage

Received: July 30, 2019  
Revised: October 2, 2019  
Published online:

- [1] J. Deane, B. O. Gallachoir, E. McKeogh, *Renew. Sustain. Energy Rev.* **2010**, *14*, 1293.
- [2] A. Smallbone, V. Jülich, R. Wardle, A. Roskilly, *Energy Convers. Manage.* **2017**, *152*, 221.
- [3] T. Fleiter, R. Elsland, M. Rehfeldt, J. Steinbach, U. Reiter, G. Catenazzi, M. Jakob, C. Rutten, R. Harmsen, F. Dittmann,

- P. Rivière, P. Stabat (2017). *Profile of Heating and Cooling Demand in 2015*. Technical Report D3.1, Heat Roadmap Europe.
- [4] J. Pacio, T. Wetzel, *Sol. Energy* **2013**, 93, 11.
- [5] J. Pacio, C. Singer, T. Wetzel, R. Uhlig, *Appl. Therm. Eng.* **2013**, 60, 295.
- [6] A. Heinzl, W. Hering, J. Kony, L. Marocco, K. Litfin, G. Mueller, J. Pacio, C. Schroer, R. Stieglitz, L. Stoppel, A. Weisenburger, T. Wetzel, *Energy Technol.* **2017**, 5, 1026.
- [7] K. Niedermeier, J. Flesch, L. Marocco, T. Wetzel, *Appl. Therm. Eng.* **2016**, 107, 386.
- [8] W. Stein, R. Buck, *Sol. Energy* **2017**, 152, 91.
- [9] K. Niedermeier, L. Marocco, J. Flesch, G. Mohan, J. Coventry, T. Wetzel, *Appl. Therm. Eng.* **2018**, 141, 368.
- [10] S. Ushak, A. Fernandez, M. Grageda, in *Advances in Thermal Energy Storage Systems*, Woodhead Publishing Series in Energy (Ed: L. F. Cabeza), Woodhead Publishing, Sawston, Cambridge UK. **2015**, pp. 49–63.
- [11] S. Hirzel, B. Sonntag, C. Rohde, *Industrielle Abwärmenutzung. Technical Report*, Fraunhofer ISE, Karlsruhe, Germany **2013**.
- [12] BCS, *Waste Heat Recovery: Technology and Opportunities in U.S. industry*. Industrial Technologies Program, US Department of Energy **2008**.
- [13] O. J. Foust, *Sodium-NaK Engineering Handbook*, Gordon & Breach, New York **1976**.
- [14] OECD-NEA, *Handbook on Lead-bismuth Eutectic Alloy and Lead Properties, Materials Compatibility, Thermal-hydraulics and Technologies*, 2 edition. OECD/NEA Nuclear Science Committee Working Party on Scientific Issues of the Fuel Cycle Working Group on Lead-Bismuth Eutectic, Issy-les-Moulineaux, France **2015**.
- [15] H. Etherington, *Nuclear Engineering Handbook*, McGraw-Hill, New York **1958**.
- [16] A. B. Zavoico, *Solar Power Tower Design Basis Document*. Technical Report SAND2001-2100, Sandia National Laboratories, Livermore, CA **2001**.
- [17] P. Li, E. Molina, K. Wang, X. Xu, G. Dehgani, A. Kohli, Q. Hao, M. H. Kassaei, S. M. Jeter, A. S. Teja, *J. Sol. Energy Eng.* **2016**, 138, 054501.
- [18] D. F. Williams, *Assessment of Candidate Molten Salt Coolants for the NNGP/NHI Heat-Transfer-Loop*. Technical Report ORNL/TM-2006/69, Oak Ridge National Laboratory, Oak Ridge, TN **2006**
- [19] X. An, J. Cheng, P. Zhang, Z. Tang, J. Wang, *Faraday Discuss.* **2016**, 190, 327.
- [20] VDI (Ed)., *VDI-Wärmeatlas*, 10., bearb. und erw. Aufl. ed, Springer, Berlin **2013**.
- [21] E.-U. Schlünder, E. Tsotsas, *Wärmeübertragung in Festbetten, Durchmischten Schüttgütern und Wirbelschichten*, Thieme, Stuttgart **1988**.
- [22] S. Ergun, *J. Chem. Eng. Progr.* **1952**, 48, 89.
- [23] M. Stieß, *Mechanische Verfahrenstechnik – Partikeltechnologie 1*, Springer, Berlin **2009**.
- [24] N. Wakao, S. Kaguei, *Topics in Chemical Engineering*, Gordon and Breach, New York **1982**.
- [25] C. Xu, Z. Wang, Y. He, X. Li, F. Bai, *Appl. Energy* **2012**, 92, 65.
- [26] M. Y. Haller, C. A. Cruickshank, W. Streicher, S. J. Harrison, E. Andersen, S. Furbo, *Sol. Energy* **2009**, 83, 1847.
- [27] M. Cascetta, G. Cau, P. Puddu, F. Serra, *Appl. Therm. Eng.* **2016**, 98, 1263.
- [28] I. Ortega-Fernández, I. Uriz, A. Ortuondo, A. B. Hernández, A. Faik, I. Loroño, J. Rodríguez-Aseguinolaza, *Int. J. Energy Res.* **2019**, 43, 6211.
- [29] J. E. Pacheco, S. K. Showalter, W. J. Kolb, *J. Sol. Energy Eng.* **2002**, 124, 153.
- [30] J.-F. Hoffmann, T. Fasquelle, V. Goetz, X. Py, *Appl. Therm. Eng.* **2016**, 100, 753.
- [31] J. I. Burgaleta, S. Arias, D. Ramirez, presented at Proc. of the 17th SolarPACES Conf. Granada, Spain, September 2011.